energies

MDPI

Article

Carbon Black–Enhanced Polyethylene Wax Phase Change Materials for Efficient Photothermal Energy Conversion and Storage in Mobile Heating Systems

Martyna Szatkowska [1], Piotr Szatkowski [1], Katarzyna Suchorowiec [1], Ewelina Radomska [2] and Kinga Pielichowska [1,*]

[1] Department of Glass Technology and Amorphous Coatings, Faculty of Materials Science and Ceramics, AGH University of Krakow, Al. Mickiewicza 30, 30-059 Krakow, Poland; szatkowska@agh.edu.pl (M.S.); pszatko@agh.edu.pl (P.S.)
[2] Department of Thermal and Fluid Flow Machines, Faculty of Energy and Fuels, AGH University of Krakow, Al. Mickiewicza 30, 30-059 Krakow, Poland; radomska@agh.edu.pl
* Correspondence: kinga.pielichowska@agh.edu.pl or kingapie@agh.edu.pl

Abstract

Organic phase change materials (PCMs) have been used and studied for many years. In this work, we focus on an industrially available PCM—polyethylene waxes (PEW) modified with seven types of carbon black (CB) exhibiting different properties. Carbon black (CB) was selected as a more cost-effective modifier compared to carbon nanomaterials, as it is easier to implement industrially and capable of converting and storing thermal energy. The experiments were designed to evaluate the thermal properties and photothermal conversion efficiency of PCMs modified with different grades of carbon black. The influence of carbon black on selected PCM properties was investigated using differential scanning calorimetry (DSC), thermogravimetric analysis (TG), scanning electron microscopy (SEM), and laser flash analysis (LFA). Furthermore, the photothermal conversion capability was evaluated. The results indicate that modification with carbon black decreases the phase transition enthalpy for most formulations, with reductions ranging from 8 to 12% for 1 wt.% CB to 10–15% for 2.5 wt.% CB. At the same time, an improvement in the thermal conductivity of PCMs modified with carbon black was observed, with the best performance achieved for N234 carbon black, showing an increase of approximately 17–18% in the 25–55 °C temperature range. The ratio of the heat of solidification to the heat of melting (Qs/Qm) for most samples was approximately 0.90–0.98, indicating excellent thermal cycling stability. The highest photothermal conversion efficiency was observed for samples modified with N234 and N330; these materials exhibited the greatest temperature rise, reaching approximately 135 °C in about 15 min, due to enhanced light absorption of PCMs by carbon black. Overall, the results confirm that PEW/CB systems demonstrate a good balance between absorption, heat generation, and controlled phase-change behavior, making them promising candidates for solar–thermal energy storage and conversion applications.

Keywords: phase-change material (PCM); carbon black; thermal analysis; photothermal conversion; thermal conductivity

Academic Editors: Paweł Czyżewski, Hao Shi and Mohammad Alnajideen

Received: 14 January 2026
Revised: 20 February 2026
Accepted: 24 February 2026
Published: 26 February 2026

1. Introduction

The rapidly growing demand for mobile heating systems, portable thermal energy storage devices, and integrated photothermal conversion applications motivates the development of optimized organic PCM formulations with enhanced thermal conductivity

and photothermal performance. Phase change materials (PCMs) constitute an attractive class of materials for thermal energy storage and energy conversion systems. PCMs store thermal energy both as sensible heat—from the initial temperature to the melting point and further to the final temperature—and as latent heat during phase transitions, such as solid–liquid or solid–solid transformations [1,2]. Compared to conventional sensible heat thermal energy storage systems, PCM-based systems offer the advantage of storing significantly larger amounts of heat within a relatively small material volume [3–5].

In general, phase change materials are classified as organic or inorganic [6]. Organic PCMs are considered chemically stable, safe, noncorrosive, and cost-effective. They are characterized by high phase transition enthalpy and good thermal reliability over numerous melting–solidification cycles [7,8]. Paraffin waxes are relatively inexpensive, safe to use, chemically inert, noncorrosive, and thermally stable up to 300 °C; however, they are flammable and exhibit low thermal conductivity (0.1–0.3 W/(m·K)). Paraffins demonstrate excellent thermal stability even after 1500 thermal cycles [8].

Paraffin- and polyethylene-based PCMs have been investigated in numerous combinations due to their structural and chemical similarities [8,9]. Zauner et al. [10] evaluated several promising polymers, including polyethylene (PE), polyoxymethylene (POM), and various polyamides (PAs), and selected high-density polyethylene (HDPE) for detailed investigation. Their results showed that HDPE exhibits a high phase transition enthalpy and remains thermally stable over more than 1000 heating–cooling cycles. The authors also designed a suitable heat exchanger, constructed a laboratory-scale storage prototype, and characterized its energy capacity and power profiles under various operating conditions. Navarro et al. [11] investigated HDPE spheres impregnated with a paraffin mixture with a melting point of 58 °C for domestic hot water applications. In their experimental system, polyethylene spheres containing embedded PCM were placed at the top of a water tank to enhance thermal stratification and increase energy density. The results demonstrated that PCM had a beneficial effect on maintaining the water temperature for an extended period. However, the presence of PE prolonged the PCM melting time as a result of its low thermal conductivity. Additionally, PCM leakage from the spheres was observed, and the PCM content would require optimization to enable safe use in drinking water tanks [11].

The primary limitation of organic PCMs is their inherently low thermal conductivity. A commonly proposed strategy to overcome this drawback is the incorporation of carbon-based additives—such as carbon black, graphene, graphite, or carbon nanotubes—to enhance heat transfer. Fikri et al. [12] proposed paraffin wax PCM with functionalized multi-walled carbon nanotubes (FMWCNTs). They reported that the addition of 1 wt.% non-functionalized MWCNTs increased thermal conductivity by 9.5%, while functionalized MWCNTs resulted in an improvement of 50.7% compared to the unmodified PCM. Feng et al. [13] investigated poly(ethylene glycol) infiltrated in porous carbon skeletons of diamond foam (DF) and dual three-dimensional carbon nanotube–diamond foam (CDF), both with a porosity of 70%. The use of DF improved thermal conductivity by 505% compared to pure PCM, whereas CDF achieved an improvement of 550%. Mishra [14] studied carbon black-modified lauric acid (LA) as a PCM. The addition of 2 wt.% carbon black increased thermal conductivity from 0.219 W/(m·K) for pure LA to 0.241 W/(m·K); a 5 wt.% loading resulted in an approximately 50% improvement compared to unmodified LA. Efforts to enhance thermal conductivity are primarily driven by the need to accelerate the PCM charging and discharging processes.

Different approaches have been investigated to enhance the thermal conductivity of PCMs. Afaynou et al. [15] proposed the use of metal foam as a partial filler in a hybrid heat sink (HS). While this strategy increases thermal conductivity, it suppresses natural convection within the PCM, thereby limiting the effective heat storage capacity

and increasing the cost of the system. N-eicosane was used as the PCM in numerical simulations. The optimal configuration was identified as two-thirds of the metal foam, resulting in a 33.82% reduction in eicosane temperature, a 12.67% increase in efficiency, a 57.54% increase in thermal energy storage, and a 33.33% reduction in the cost and weight compared to a fully filled metal foam configuration [15]. Mishra et al. [16] proposed the incorporation of lauric acid modified with 4 wt.% carbon black nanoparticles or 4 wt.% graphene nanoplatelets into a biomass-derived porous matrix obtained from coffee or turmeric powder. The incorporation of 25 wt.% of the porous matrix significantly improved structural stability by effectively suppressing PCM leakage while maintaining a high latent heat storage capacity of approximately 130 J/g. Solid–solid composite PCMs exhibited high photothermal conversion efficiency (106%) and notable thermal regulation capability, reducing the superheating temperature by approximately 10 °C compared with the pristine PCM. These enhancements were attributed to improved light absorption and increased energy conversion efficiency [16]. The thermal conductivity in organic PCMs can also be improved by incorporating boron nitride, as demonstrated by Yu et al. [17]. The authors constructed thermally conductive boron nitride (BN) networks within a paraffin wax (PW) matrix supported by poly(styrene-b-ethylene-butylene-b-styrene) (SEBS). The composite with a 20/80 SEBS to PW mass ratio and containing 30 wt.% BN exhibited excellent dimensional stability, a high latent heat capacity (129.8 J/g), and significantly enhanced thermal conductivity of 1.51 W/(m·K), representing a 293% increase compared to the unfilled material [17].

Despite the superior thermal enhancements achievable with carbon nanomaterials, carbon black represents a more cost-effective and industrially viable alternative for PCM modification. In this work, polyethylene waxes modified with seven distinct types of carbon black were investigated. The influence of carbon black properties, such as particle size, specific surface area, and conductivity characteristics, on thermal behavior, thermal conductivity, and photothermal performance was systematically assessed. The resulting materials were characterized using differential scanning calorimetry (DSC), thermogravimetric analysis (TG), scanning electron microscopy (SEM), laser flash analysis (LFA), and photothermal conversion measurements.

In this work, polyethylene waxes modified with seven distinct types of carbon black with different parameters and characteristics were investigated. The influence of carbon black properties, such as particle size, specific surface area, and conductivity, on thermal behavior and thermal conductivity to find structure–properties relationships, has been investigated. Moreover, photothermal performance was systematically assessed to identify the most effective CB grades for solar–thermal energy conversion and storage applications and mobile heating.

2. Materials and Methods

The polyethylene waxes (PEW) were obtained from EuroCeras Sp. z o.o. (Cerelane 1100, Kędzierzyn Koźle, Poland), carbon black N220, N330, N234, conductive (Konin, Poland), carbon black HCS-2, HCS-165, HCS-200S (Hangzhou, China)—Table 1.

Samples of PEW were heated at a temperature of 130 °C to melting, then 1, 2.5, and 5% of modifiers (carbon blacks) were added to the melted PEW and homogenized using an ultrasonic homogenizer to obtain a homogenous dispersion. Homogenization time was 30 s. It was observed that too long a homogenization process generates intense heat and significantly reduces the efficiency of the process by causing excessive cavitation. The material designations used in the tests are described in Table 2.

Table 1. Properties of CBs.

Carbon Black	Particle Size [nm]	Total Specific Surface [10^3 m^2/kg]	Ash (Mass Fraction) [%]
N220	20–25	101–111	0.50
N330	26–30	107–117	0.50
N234	19–23	70–80	0.50
conductive	20–50	65.0 ± 5.0	0.50
HCS-2	20–25	200–600	≤0.50
HCS-165	16	80–200	≤0.20
HCS-200S	24–28	150–300	≤0.50

Table 2. Samples description.

Sample	Name Used in the Article	CB Content [%]
PEW	PCM	-
PEW + electroconductive carbon black	PCM+E_CB	1.0 2.5 5.0
PEW + carbon black N220	PCM+CB_N220	1.0 2.5 5.0
PEW + carbon black N234	PCM+CB_N234	1.0 2.5 5.0
PEW + carbon black N330	PCM+CB_N330	1.0 2.5 5.0
PEW + carbon black HCS2	PCM+CB_HCS2	1.0 2.5 5.0
PEW + carbon black HCS165	PCM+CB_HCS165	1.0 2.5 5.0
PEW + carbon black HCS200	PCM+CB_HCS200	1.0 2.5 5.0

Differential scanning calorimetry (DSC) measurements were conducted using the DSC 1 calorimeter from Mettler Toledo (Greifensee, Switzerland), equipped with an intracooler. Prior measurements, DSC was calibrated with indium and zinc standards. The temperature program involved a heating–cooling–heating cycle within a temperature range of 25 to 130 °C, with a heating and cooling rate of 10 °C/min in a nitrogen atmosphere (30 mL/min). Samples with mass ca. 3 mg were closed in pierced aluminum pans. The first heating run was performed for the removal of the samples' thermal history resulting from the preparation and processing.

Additionally, DSC 1 was utilized for modulated temperature DSC measurements in TOPEM mode, with parameters set at an amplitude of 0.5 K, a switching time of 15 s, and a base heating rate of 1 K/min over the temperature range of 25 to 130 ° C.

Additionally, DSC250 from TA Instruments (New Castle, DE, USA), was used, which featured a refrigerated cooling system to analyze the phase change material after 20 cycles

of heating–cooling within a temperature range of 25 to 130 °C, with a rate of 10 °C/min in a nitrogen atmosphere (340 mL/min).

Fourier transform infrared (FTIR) measurements were performed using a spectrophotometer from ThermoFisher Scientific (Waltham, MA, USA) model: Nicolet iS20 Nicolet Apex with an Attenuated Total Reflection (ATR) adapter, operating with OMNIC 9.16.188 software. Spectra were collected in absorbance mode of 4000–400 cm^{-1} after 32 scans at 4 cm^{-1}.

Thermogravimetric analyses were performed using a TGA 550 Discovery analyzer (TA Instruments, New Castle, DE, USA). The samples were examined in a temperature range of 40–600 °C, with a heating rate of 10 K/min under a nitrogen atmosphere.

Scanning electron microscopy (SEM) was carried out using a NOVA NANO SEM 200 system (FEI, Hillsboro, OR, USA) equipped with EDS. Before imaging, the sample was coated with a carbon layer and examined at magnifications of approximately 2000× and 10,000×.

Thermal diffusivity was measured using the laser flash analysis (LFA) method with an LFA 467 HyperFlash instrument (Netzsch, Selb, Germany). All measurements were performed in an inert nitrogen atmosphere with a gas flow rate of 50 mL/min. The tests were carried out at 25 °C, 40 °C, 55 °C, and 70 °C (solid state). For each temperature, the chamber was first stabilized, followed by a 300 s equilibration period before the laser pulse to ensure uniform temperature throughout the sample. Three measurements were carried out at each temperature step. The samples were cylindrical (height: 1.55 mm; diameter: 15 mm) and placed in a holder, externally secured with stainless-steel spacers coated with graphite, as shown in Figure 1. Heating was carried out at 5 K/min to the target temperature, after which a laser pulse of known energy was applied. From the moment of irradiation, the temperature response on the rear surface of the sample was recorded. The resulting signals were analyzed using LFA Proteus 8.0.3 software, and thermal diffusivity was determined using the selected three-layer model. Then, the thermal conductivity (λ, W/(m·K)) was calculated as follows:

$$\lambda = \alpha \rho c_p \tag{1}$$

where α, ρ, and c_p stand for thermal diffusivity (mm^2/s), density (g/cm^3), and specific heat capacity (J/g). The density was determined from the Archimedes method, while the specific heat capacity was obtained from the DSC measurements. The uncertainty of the thermal conductivity was estimated from the general formula for error propagation [18]:

$$\delta\lambda = \sqrt{\left(\frac{\partial\lambda}{\partial\alpha}\delta\alpha\right)^2 + \left(\frac{\partial\lambda}{\partial\rho}\delta\rho\right)^2 + \left(\frac{\partial\lambda}{\partial c_p}\delta c_p\right)^2} \tag{2}$$

where δ stands for the uncertainty of a specific variable. According to the producers, the uncertainties of $\delta\alpha$, $\delta\rho$, and δc_p are 3% [19], 0.4% [20], and 2% [21], respectively. Thus, the estimated uncertainty of the thermal conductivity is 3.6%.

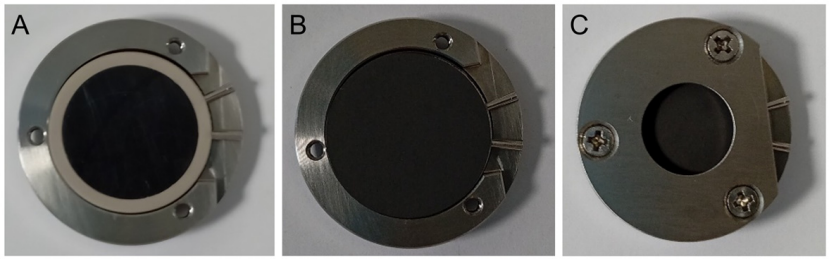

Figure 1. A sample during the preparation for the LFA measurements: (**A**) the sample in a PEEK ring; (**B**) the sample secured with a graphite-coated stainless-steel spacer; (**C**) the complete measurement holder.

The photothermal conversion performance was investigated using the LED Ossila Solar Simulator (Ossila, Sheffield, UK), with a light spectrum ranging from 350 to 1050 nm at a working distance of 8.5 cm and output power of 1 Sun for 36 min at room temperature. Following the experiment, the samples were placed in a customized experimental setup for photothermal conversion evaluation according to Figure 2.

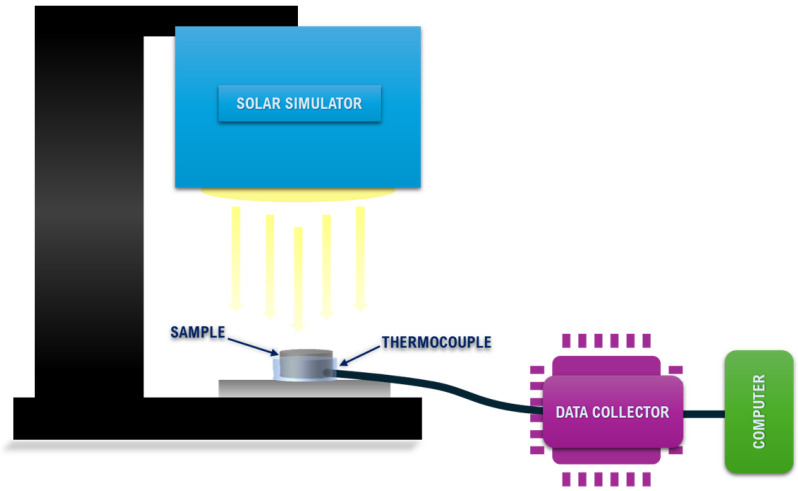

Figure 2. Scheme of the experimental setup for photothermal conversion evaluation.

The temperature of the sample was recorded through a thermocouple connected with a PicoLog TC-08 high-resolution thermocouple data logger (Pico Technology, St Neots, UK) connected to the computer. The temperature of the sample was recorded during the exposition to the simulated solar light and when the simulated solar source was switched off. When the experiment (solar exposition) time reached 36 min, the simulated solar light source was turned off, allowing the sample to cool down naturally to the room temperature. The photothermal conversion efficiency was calculated following Equation (3) [22–24]:

$$\eta = \frac{m \cdot \Delta H_m}{I \cdot S \cdot (T_e - T_s)} \cdot 100\% \quad (3)$$

where η denotes the photothermal conversion efficiency; m is the mass of the phase-change material (PCM); ΔH represents the enthalpy of the PCM; I corresponds to the optical power density (1000 W/m^2); S denotes the irradiated surface area; T_s is defined as the onset time of the phase transition, and T_e is defined as the termination time of the phase transition.

3. Results and Discussion

To evaluate the material's ability to absorb and release heat, DSC measurements were performed using a heating–cooling–heating cycle. Data from the second heating run were analyzed, as the first run was used to eliminate the thermal history of the samples. The DSC results are presented in Figure 3 and Table 3.

The addition of carbon black only slightly affects the shifts in melting or crystallization peaks. The differences are typically around one degree between the pure PCM and the modified sample. There is no clear relationship between the temperature changes in individual peaks and either the carbon black content or the specific type of carbon black used.

Phase transition temperatures are intensive properties of the polyethylene wax matrix phase, determined exclusively by molecular composition and thermodynamic equilibrium. The physical dispersion of non-interacting carbon black cannot alter this intrinsic thermodynamic property. Consistent values of Tm and Ts across all formulations (95–96 °C and 90–91 °C, respectively) thus demonstrate strong thermal compatibility and the absence of interfacial chemical reactions, as it was confirmed in FTIR results.

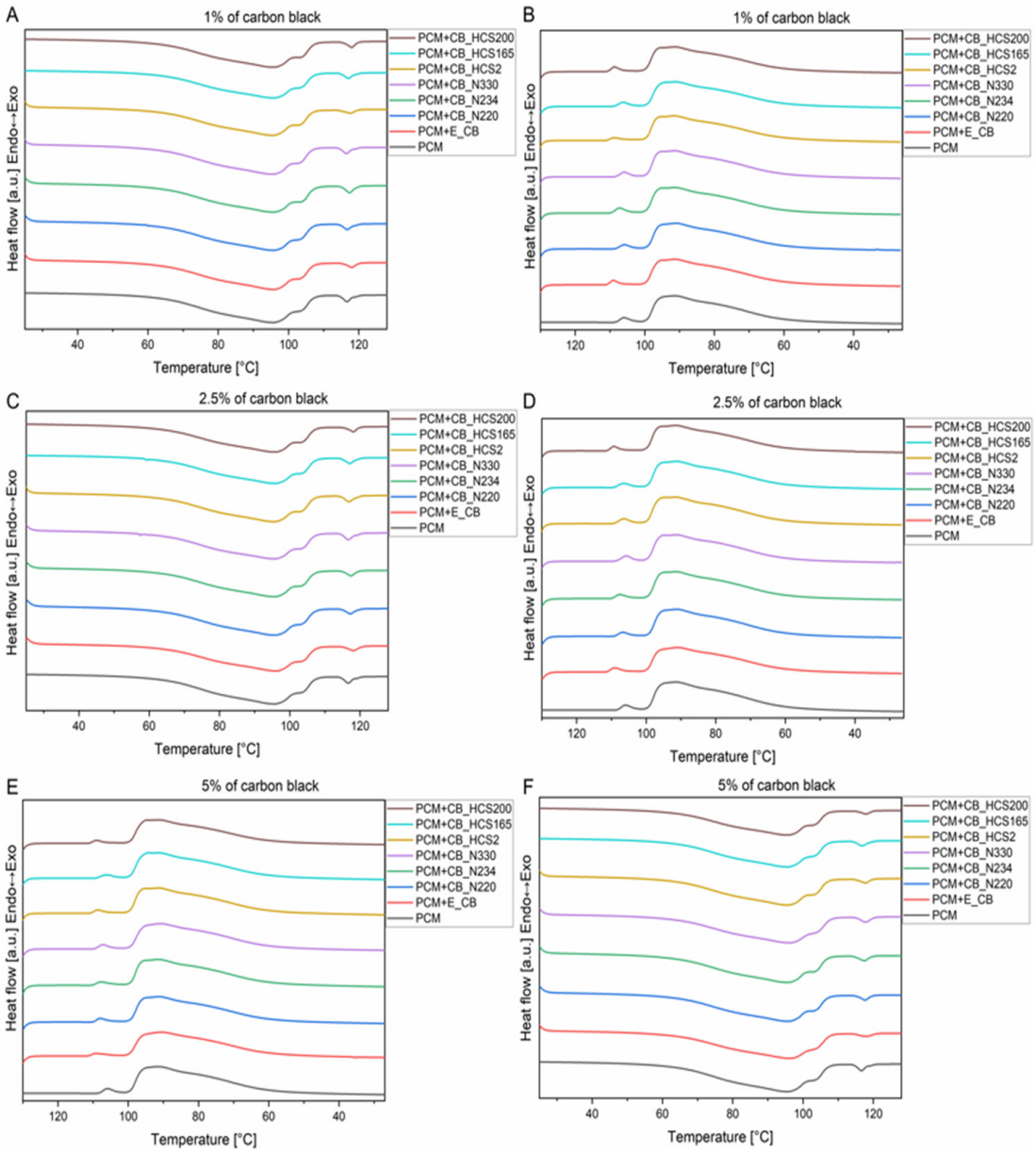

Figure 3. DSC curves for PCM with carbon black 1% (**A**,**B**), 2.5% (**C**,**D**), and 5% (**E**,**F**), and heating (**A**,**C**,**E**) and cooling (**B**,**D**,**F**).

Table 3. Temperature and heat of melting and solidification of PCM/CB (Q_m—the heat of fusion, Q_s—the heat of solidification).

Sample	CB Content [%]	T_{monset} [°C]	T_{m1} [°C]	T_{m2} [°C]	T_{m3} [°C]	Q_m [J/g]	T_{sonset} [°C]	T_{s1} [°C]	T_{s2} [°C]	T_{s3} [°C]	Q_s [J/g]
PCM	-	62	95	104	117	242.84	99	106	91	77	242.57
PCM+E_CB	1	62	96	104	118	227.39	100	109	91	77	226.53
	2.5	62	96	104	118	213.67	100	109	91	77	210.68
	5	62	96	104	115	214.51	100	109	90	77	213.35
PCM+CB_N220	1	62	96	104	115	227.85	99	106	91	77	224.50
	2.5	62	96	104	115	223.42	99	107	91	77	218.22
	5	62	96	104	118	221.30	99	108	91	77	217.18

Table 3. *Cont.*

Sample	CB Content [%]	T_{monset} [°C]	T_{m1} [°C]	T_{m2} [°C]	T_{m3} [°C]	Q_m [J/g]	T_{sonset} [°C]	T_{s1} [°C]	T_{s2} [°C]	T_{s3} [°C]	Q_s [J/g]
PCM+CB_N234	1	62	96	104	117	232.38	100	109	91	78	227.52
	2.5	62	95	104	117	223.83	99	108	91	78	219.19
	5	62	96	103	117	225.84	99	108	91	77	221.03
PCM+CB_N330	1	61	95	103	116	230.08	99	108	91	78	226.09
	2.5	62	95	104	117	222.77	100	106	91	78	218.20
	5	62	96	104	118	228.82	99	107	90	78	225.92
PCM+CB_HCS2	1	62	95	104	118	219.85	100	109	92	77	215.24
	2.5	62	95	104	117	223.97	100	106	91	78	219.02
	5	62	96	103	118	223.64	100	109	91	77	219.79
PCM+CB_HCS165	1	62	96	104	117	219.93	99	106	91	77	220.36
	2.5	62	96	104	117	221.89	99	107	91	76	222.42
	5	62	95	104	117	222.82	99	106	91	78	222.96
PCM+CB_HCS200	1	62	96	104	118	226.13	100	109	91	77	226.55
	2.5	61	96	104	118	223.60	100	109	91	78	223.60
	5	62	95	104	118	212.93	99	109	91	77	213.20

In contrast, enthalpy values are extensive properties directly proportional to the mass of active phase change material in the composite. The observed enthalpy reductions (8–15%) result from: (i) effective PCM mass reduction due to space occupancy by carbon black (~1% for 1 wt.% loading), (ii) crystallization hindrance caused by CB particles, (iii) surface-mediated perturbation of local crystal order. This combined effect stay with good agreement with the literature data on carbon-modified paraffin systems and represents an optimized engineering trade-off: accepting modest enthalpy reduction in exchange for substantial thermal conductivity improvement (up to 22% for optimal CB grades) [25–27]. This strategy enables faster energy transfer during charging/discharging cycles, partially compensating for lower absolute storage capacity per unit mass.

The latent heat of fusion represents the thermal energy storage capacity of a material and is directly measured by DSC. For the pure PCM, the heat of melting was 242.84 J/g, which is characteristic of paraffin-based PCMs. Modification with carbon black leads to a systematic decrease in enthalpy across most formulations [28], ranging from 8 to 12% for 1 wt.% CB to 10–15% for 2.5 wt.% CB. The reduction in melting heat with increasing CB content is consistent with reports in the literature on nanoparticle-enhanced PCMs. Studies on carbon-modified paraffin systems have demonstrated similar trends, in which the addition of carbon-based fillers—such as carbon nanotubes, graphene, or activated carbon—results in a slight decrease in latent heat capacity [29–31]. In general, for polymer-based PCMs, the thermal energy storage capacity is directly connected to the degree of crystallinity. The incorporation of micro- or nanometric-sized additives leads to changes in the polymer matrix crystallization process. Depending on the type, size, shape, chemical composition, and concentration, incorporated additives have different effects on the crystallization process. Polymer chains can interact with fillers by chemisorption or occlusion, that trigger the macromolecule nucleation process [32]. In the most widely accepted paracrystalline model for different types of carbon black, continuous layers of hexagonally arranged carbon atoms form the basic building blocks. These carbon layers are concentrically arranged around one or more growth nuclei, resulting in adjacent layers orientated parallel to each other and

creating ordered, parallel stacked layers known as a turbostratic structure, and finally forming nearly spherical particles and aggregates [33]. In polymer systems, paracrystalline CB structures can act as nucleating sites for polymer chains; however, the opposite confinement effect may also influence the crystallization ability of PEW. The mobility of PEW polymer chains can be restricted because of chain trapping within the narrow spaces between CB particles or adsorption onto high surface-area CB particles, which limits the crystallization process of PEW. This leads to a decrease in PEW crystallinity and a reduction in the heat of phase transition of the PCM system. The reduction in phase change enthalpy can also be attributed to a decrease in the effective PCM volume fraction within the composite, as carbon black nanoparticles occupy space in the material and thereby reduce the mass fraction of active PCM available for thermal energy storage [34–36]. However, the magnitude of the decrease (8–15%) is relatively modest, suggesting good compatibility between the carbon black particles and the PEW matrix. Previous studies on paraffin composites containing various carbon-based nanofillers have reported comparable or even larger enthalpy reductions (ranging from 3 to 40%, depending on filler type and concentration), indicating that the carbon black modifications applied in this study preserve thermal storage capacity to a satisfactory extent [37,38].

The solidification temperature (Ts) remained constant at 90–91 °C for all samples during the cooling cycle, demonstrating excellent thermal reversibility. This consistency is particularly important for applications requiring long-term cycling stability, as it indicates reliable phase transitions during repeated thermal cycles. The heat of solidification (Qs) ranged from 210 to 227 J/g and closely matched the corresponding melting enthalpy values, further confirming the reversibility of the phase transitions and the absence of significant material degradation during DSC measurements. The ratio of the heat of solidification to the heat of melting (Qs/Qm) for most samples was approximately 0.90–0.98, indicating excellent thermal cycling behavior. This observation is supported by literature on paraffin-based PCMs, where similar ratios have been reported for properly functioning phase change materials. Minor asymmetries between melting and crystallization enthalpies are common and can be attributed to nucleation effects and slight differences in heat transfer rates during heating and cooling cycles [39,40].

The melting temperatures observed in this study (95–96 °C) and the corresponding latent heats (212–243 J/g) are consistent with the reported values for paraffin waxes used as phase change materials. The literature data for standard paraffin PCMs with comparable melting points typically indicate latent heats in the range of 200–280 J/g. Polyethylene wax used in this work represents a mid-range paraffin formulation, and the measured thermal properties align well with those of commercially available PCM products and other paraffin-based thermal energy storage materials [41,42].

The influence of carbon black on the melting temperature was minimal, which contrasts with some reports from the literature that describe temperature shifts of ±2–5 °C upon the addition of certain nanofillers. This thermal stability is advantageous for mobile heating system applications, as it ensures consistent operating temperatures regardless of the specific carbon black formulation used [43].

Based on the obtained data, the relationship between the specific surface area (SSA) of CB and the investigated parameters can be found. In general, better results have been revealed for CB with lower SSA. Samples with carbon black N330 and N234 were characterized by slightly higher phase transition. Based on DSC data, the degree of crystallinity of the PEW matrix has been calculated to check the effect of SSA and the crystallinity of the polymer matrix—Figure 4.

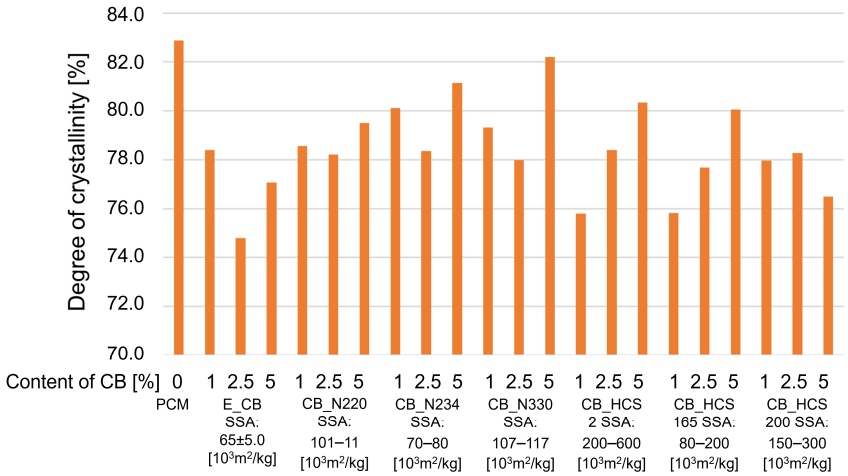

Figure 4. Degree of crystallinity of PEW vs. carbon black SSA and content [%].

From Figure 4 can be seen that in such systems polymer matrix can reach a slightly higher degree of crystallinity in systems modified with CB, characterized by lower SSA.

In Table 4 we shown DSC results after 20 heating–cooling cycles for the PCM base material and the two best formulations revealed that the best thermal behavior and repeatability were exhibited by the PCM+CB_N330 sample, where the values of heat of phase transition were on a similar level as before thermal cycling. For unmodified PCM and PCM+CB_N234, some decrease in phase transition enthalpy was found, but the obtained values are still above 200 J/g.

Table 4. DSC results after 20 heating–cooling cycles.

Sample	CB Content [%]	T_{monset} [°C]	T_{m1} [°C]	T_{m2} [°C]	T_{m3} [°C]	Q_m [J/g]	T_{sonset} [°C]	T_{s1} [°C]	T_{s2} [°C]	T_{s3} [°C]	Q_s [J/g]
PCM	-	63	97	105	115	204.38	98	102	89	76	209.42
PCM+CB_N330	1	64	96	103	116	231.63	98	104	89	76	217.09
PCM+CB_N234	1	63	97	104	117	208.00	98	104	89	76	208.25

Analysis of the FTIR results for both neat PCM, PCM/CB samples, and CB indicates no changes in PEW in the presence of carbon black, which indicates no chemical reaction between the PCM and the carbon additive (Figures 5 and 6).

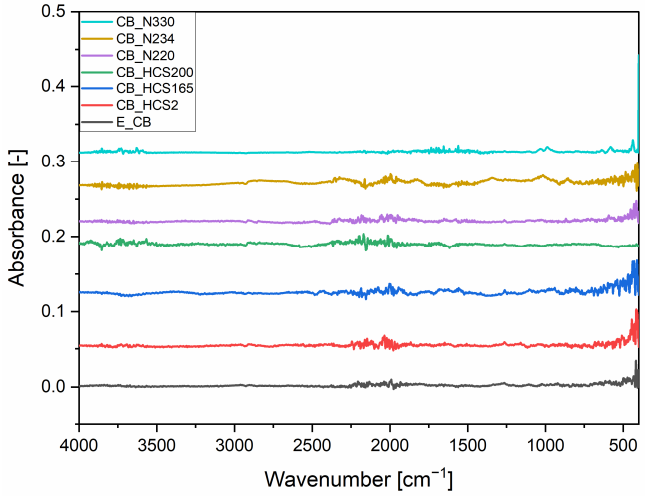

Figure 5. FTIR spectra of carbon black.

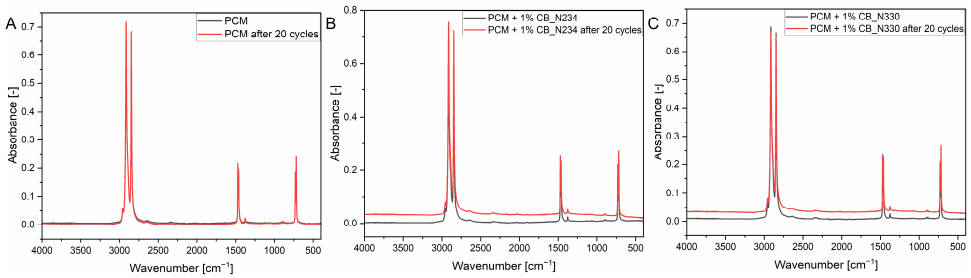

Figure 6. FTIR spectra of PCM before and after 20 heating–cooling cycles (**A**), PCM + 1% CB_N234 before and after 20 heating–cooling cycles (**B**), PCM + 1% CB_N330 before and after 20 heating–cooling cycles (**C**).

There are no characteristic absorption bands in the spectrum that could be associated with functional groups in carbon black. Only absorption bands typical for polyethylene wax were found (at 718 and 730 cm^{-1} from CH_2 rocking vibration [44], at 1462 and 1472 cm^{-1} from CH_2 bending [45], at 2847 and 2914 cm^{-1} from C-H stretching in alkanes [46]. Moreover, Fourier transform infrared spectroscopy analysis has been performed for samples after 20 thermal cycles and showed that the PCM before phase transitions and after 20 phase transition cycles (20 heating–cooling cycles) exhibits peaks originating from chemical bonds at the same positions and with the same intensities as before thermal cycling. In the same figure, we can see that a similar relationship is observed for samples modified with one percent of carbon black in B-CB 234 and in C-CB-330.

The thermal stability of the carbon black modified PCMs was further evaluated by thermogravimetric (TG) analysis; the results are presented in Table 5 and Figure 7.

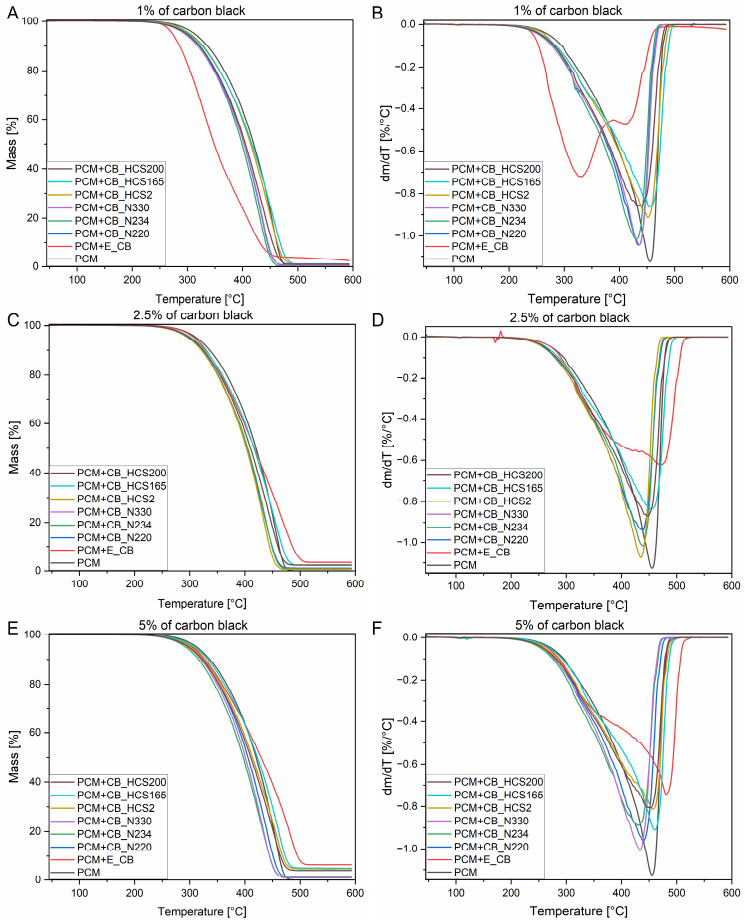

Figure 7. TG (**A**,**C**,**E**) and DTG (**B**,**D**,**F**) curves for PCM (Cerelane 1100) with carbon black 1% (**A**,**B**), 2.5% (**C**,**D**), and 5% (**E**,**F**).

The unmodified PEW exhibited excellent thermal stability, with the onset of mass loss ($T_{1\%}$) occurring at 267 °C. This high initial decomposition temperature ensures safe operation in heating applications up to moderate temperatures. The temperature corresponding to 10% mass loss ($T_{10\%}$) was 336 °C, while the temperature at 50% mass loss ($T_{50\%}$) reached 420 °C, indicating a relatively broad window of thermal stability. The maximum decomposition rate (T_{DTGmax}) occurred at 462 °C. The residual char at 600 °C was negligible (0.002%), confirming nearly complete decomposition of the organic paraffin material at elevated temperatures. These values are in excellent agreement with the data from the literature for paraffin waxes. Studies on conventional paraffin-based PCMs typically report $T_{10\%}$ values in the range of 300–350 °C and $T_{50\%}$ values between 400 and 450 °C, indicating that the PEW formulation used in this study is representative of commercially available paraffin products [42,47].

Table 5. Thermal stability of PCM with carbon black.

Sample	CB Content [%]	$T_{1\%}$ [°C]	$T_{2\%}$ [°C]	$T_{3\%}$ [°C]	$T_{5\%}$ [°C]	$T_{10\%}$ [°C]	$T_{50\%}$ [°C]	T_{DTGmax} [°C]	Char Residue at 600 °C [%]
PCM	-	267	285	297	312	336	420	462	0.002
PCM+E_CB	1	251	260	265	273	286	348	328	2.405
	2.5	269	286	296	309	330	417	475	3.432
	5	263	280	291	305	328	429	481	6.344
PCM+CB_N220	1	257	274	284	299	321	403	431	0.754
	2.5	259	275	285	299	322	404	440	1.093
	5	258	275	286	301	324	406	440	1.026
PCM+CB_N234	1	257	273	284	299	321	399	431	0.143
	2.5	255	271	282	298	321	405	441	0.859
	5	250	267	278	293	316	397	426	0.882
PCM+CB_N330	1	252	269	280	295	319	403	436	0.507
	2.5	255	272	283	298	322	403	433	0.654
	5	257	273	283	298	321	401	433	1.105
PCM+CB_HCS2	1	265	280	290	305	329	415	452	1.135
	2.5	260	278	289	304	329	415	451	2.269
	5	258	275	286	301	326	414	456	4.62
PCM+CB_HCS165	1	258	275	286	302	327	417	454	1.111
	2.5	259	276	288	303	328	416	452	2.276
	5	261	280	292	308	333	423	460	4.943
PCM+CB_HCS200	1	253	271	282	298	322	405	440	0.961
	2.5	258	274	285	300	325	410	450	2.365
	5	253	271	282	298	323	411	451	3.941

The addition of carbon-black nanoparticles has a complex, nonuniform effect on thermal stability:

- Electroconductive carbon black (E_CB) exhibited the most pronounced influence on thermal decomposition behavior. At a 1 wt.% loading, the onset temperature of mass loss ($T_{1\%}$) decreased to 251 °C, while at higher loadings it increased to the range of 263–269 °C. The temperatures corresponding to 50% mass loss ($T_{50\%}$) varied between 348 and 429 °C, depending on the concentration of carbon black. In particular, this

formulation showed the highest char residue at 600 °C (2.405–6.344%), indicating incomplete decomposition and the possible accumulation of carbonaceous residue. This behavior can be attributed to the presence of conductive carbon black particles, which do not fully decompose and remain as stable carbon-rich residues at elevated temperatures.

- Carbon black grades N220, N234, and N330 exhibited more moderate effects on the thermal stability of PEW. The onset temperatures of mass loss ($T_{1\%}$) ranged from 250 to 257 °C at a 1 wt.% loading, while the temperatures corresponding to 50% mass loss ($T_{50\%}$) remained relatively stable at 399–406 °C, only slightly lower than those of the pure PCM. The char residue for these formulations was minimal (0.143–1.105%), indicating more complete thermal degradation compared to electroconductive variants. This behavior, which closely resembles that of the unmodified PCM, suggests that conventional carbon black grades exhibit good thermal compatibility with paraffin-based matrices [48,49].
- Carbon Black HCS series: The HCS formulations (HCS2, HCS165, and HCS200) exhibited an intermediate influence on the thermal stability of PEW. The onset temperatures of mass loss ($T_{1\%}$) ranged from 253 to 265 °C, while the temperatures at 50% mass loss ($T_{50\%}$) were between 405 and 423 °C, remaining very close to the pure PCM baseline. The char residue at 600 °C varied from 0.961 to 4.943%, which is higher than that observed for standard carbon black grades but lower than for electroconductive variants. This behavior suggests that specialty carbon black grades may form more thermally stable interactions with the paraffin matrix, contributing to enhanced thermal resistance at elevated temperatures.

The observed thermal behavior can be understood in the context of carbon-paraffin interactions. Studies on PCMs enhanced with carbon nanoparticles have demonstrated that carbon additives can enhance or slightly reduce thermal stability depending on their surface properties and degree of dispersion [34,35].

The reduction in $T_{1\%}$ (initial decomposition temperature) observed in this study stay with good agreement with literature findings. Research on graphene-enhanced paraffin systems reported $T_{1\%}$ reductions of 5–15 °C compared to pure paraffin, similar to the 8–16 °C reduction observed with carbon black in this study. This phenomenon is attributed to surface-catalyzed decomposition, where the high surface area of nanoparticles can catalyze the thermal decomposition of nearby paraffin molecules at lower temperatures [48–50].

The formation of a carbonaceous residue (char) at elevated temperatures is a characteristic feature of carbon-filled composites. The increase in char residue with increasing carbon black content observed in this study follows the expected trend: for a composite containing N wt.% of non-decomposable carbon black, the theoretical char yield should approach N wt.%. However, the experimentally observed values (0.002–6.344%) are generally lower than the nominal carbon black loadings (up to 5 wt.%), suggesting partial pyrolysis of carbon black into gaseous products and/or interactions with paraffin decomposition products. Previous studies on the thermogravimetric behavior of carbon-filled polymers indicate that char formation at 600 °C may account for 40–100% of the initial carbon black content, depending on the carbon black grade and thermal processing conditions. The relatively low char yields observed in this work—particularly for standard carbon black grades—suggest good dispersion and integration of carbon black within the paraffin macromolecular structure, as well as possible partial degradation of the carbon filler under the applied measurement conditions [48].

For applications in mobile heating systems, the thermal stability demonstrated by all formulations is excellent. According to the DSC results, the melting point was determined at ca. 90–96 °C, well below the $T_{1\%}$ values (251–269 °C) observed in TG analysis. This

margin ensures that these PCM will maintain their thermal storage functionality throughout the design life of mobile heating systems that operate in typical temperature ranges (up to 60–100 °C) [41].

The observed carbon black aggregate sizes (in the range of 100–500 nm) are consistent with those of industrial carbon black products commonly used in thermal and electrical applications. Literature on carbon black nanostructure indicates that commercial carbon blacks consist of primary particles aggregated into larger structures, with aggregate sizes typically ranging from tens of nanometers to several micrometers, depending on the manufacturing process. The size range identified in this study places carbon black within the nanoparticle regime, which is advantageous for achieving property enhancement while maintaining adequate dispersion stability [51]. The uniformity of particle distribution observed at the micrometer scale compares favorably with reports on other nanoparticle–polymer systems. Studies on graphene oxide–paraffin and carbon nanotube–paraffin composites frequently describe localized agglomeration and clustering, particularly at higher filler loadings. The superior dispersion observed in the present carbon black–based systems may be attributed to the spherical or near-spherical morphology of carbon black aggregates, which pack more efficiently than the highly anisotropic structures of carbon nanotubes or graphene sheets [34,52,53].

For mobile heating system applications, the microstructural characteristics revealed by SEM analysis are highly advantageous. The homogeneous distribution of carbon black throughout the paraffin matrix ensures uniform material properties, which are critical for reliable thermal energy storage and heat transfer. In addition, good interfacial contact between the filler and the matrix reduces thermal resistance at the particle–matrix interfaces, which would typically be expected to enhance thermal conductivity. However, the LFA results indicate an unexpected decrease in thermal conductivity, suggesting that other effects—such as particle-induced phonon scattering or disruption of the paraffin crystalline structure—may dominate over the benefits of improved interfacial contact in this system [54].

Figure 8 shows SEM images of carbon black modified samples, and Figure 9 also shows EDS analysis.

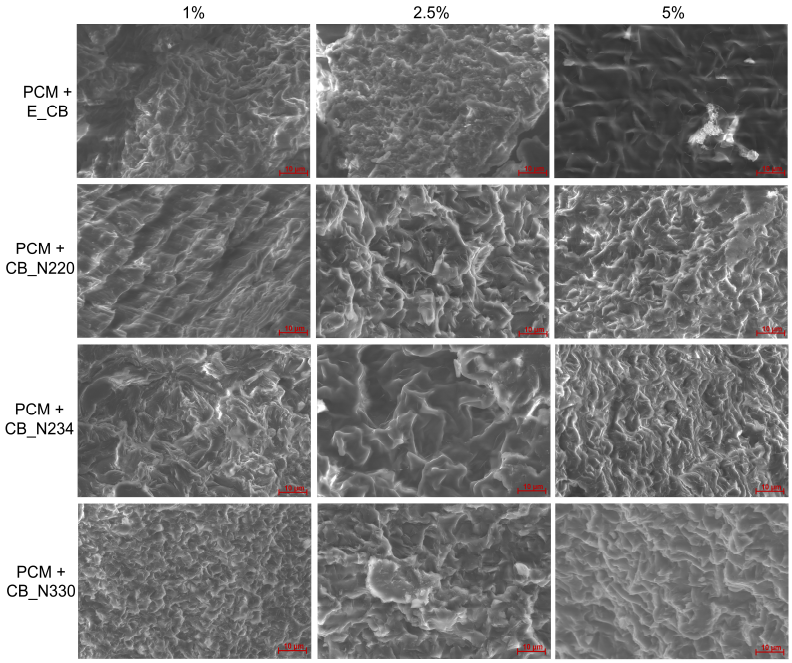

Figure 8. SEM 5000× images of PCM + 1%, 2.5%, 5% E_CB (**first row**) PCM + 1%, 2.5%, 5% CB_N220 (**second row**), PCM + 1%, 2.5%, 5% CB_N234 (**third row**), and PCM + 1%, 2.5%, 5% CB_N330 (**forth row**).

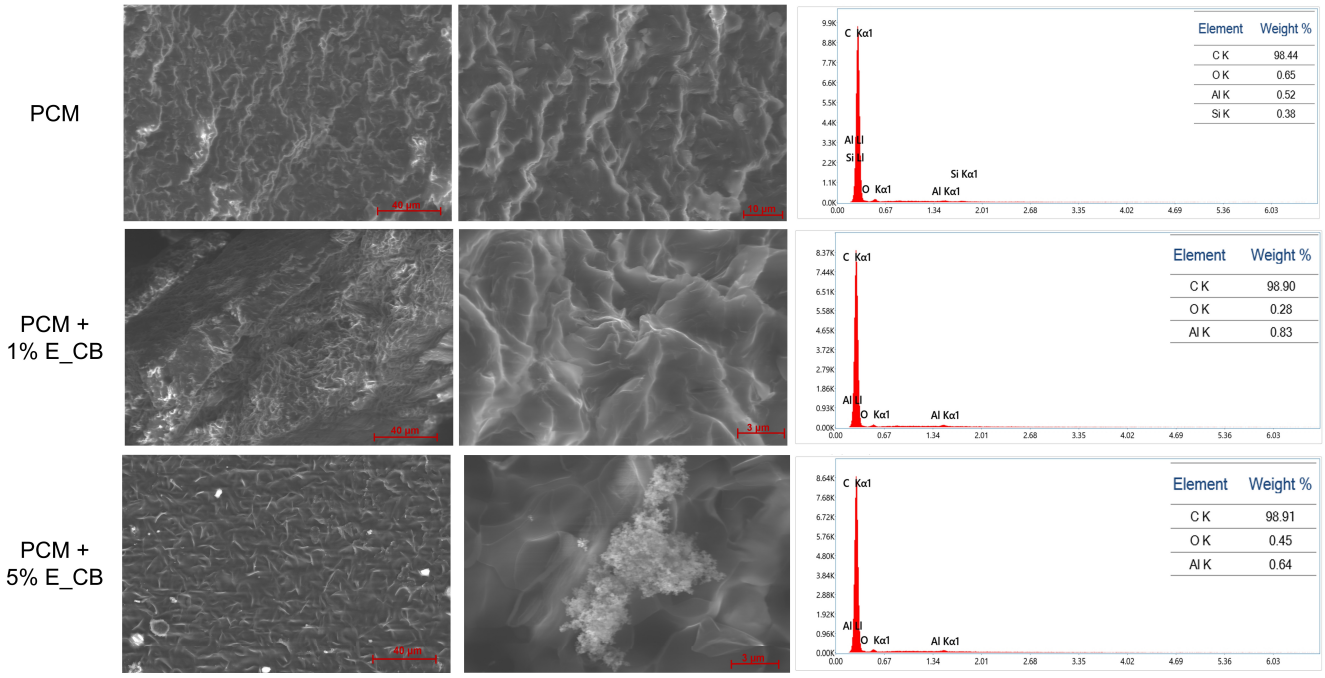

Figure 9. SEM images, from left to right respectively: PCM 2000×, 5000×, EDS (**first row**) PCM + 1% E_CB 2000×, 10,000×, EDS (**second row**), PCM + 5% E_CB 2000×, 10,000×, EDS (**third row**).

The absence of pronounced agglomeration or clustering in the SEM images further suggests that the composites are likely to maintain microstructural integrity during repeated thermal cycling. Such stability is essential for the durability and long-term reliability of phase change materials subjected to multiple heating and cooling cycles. Previous studies on PCM composites have emphasized the importance of microstructural stability in preserving long-term performance [55].

Figure 10 shows graphs of the specific heat capacity obtained using TOPEM DSC measurements. During phase transitions, the specific heat is highest [56]. Additionally, the highest heat of fusion is observed for materials with the highest carbon black content.

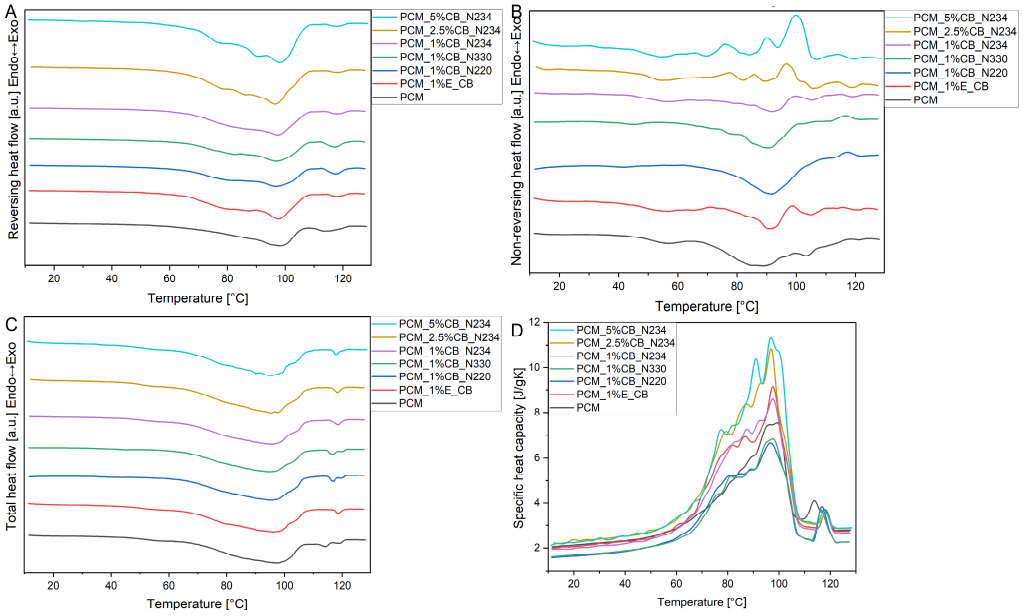

Figure 10. TOPEM DSC results: (**A**) reversing heat flow curves, (**B**) non-reversing heat flow curves, (**C**) total heat flow curves of TPCMs mixtures, (**D**) specific heat capacity curves of PCM with carbon black mixtures.

Figure 10 shows that the reversing heat flow curves (A) indicate melting during heating as a reversible process. In contrast, the non-reversing heat flow (B) exhibits exothermic signals associated with recrystallization, followed by a peak corresponding to complete melting (C). Samples with higher carbon black mass fractions show a greater extent of recrystallization, which leads to an increased number of crystal defects. As a result, the enthalpy of the phase transition may be reduced. Overall, the heat flow profiles closely resemble those obtained from conventional DSC measurements. The specific heat capacity (C_p) values were determined from the TOPEM DSC measurements. The results of the thermal conductivity measurements were calculated using Equation (1) and are presented in Table 6.

Table 6. Results of thermal diffusivity and thermal conductivity of PCM with carbon black.

Sample	Thermal Diffusivity, mm^2/s				Thermal Conductivity, W/(m·K)			
	Temperature, °C				Temperature, °C			
	25	**40**	**55**	**70**	**25**	**40**	**55**	**70**
PCM	0.1480	0.1345	0.1180	0.0915	0.3030	0.2930	0.2950	0.3095
PCM + 1% CB_N234	0.1675	0.1475	0.1275	0.0930	0.3235	0.3090	0.3140	0.3620
Percentage improvement, %	13.2	9.7	8.1	1.6	6.8	5.5	6.3	17.0
PCM + 2.5% CB_N234	0.1570	0.1400	0.1200	0.0900	0.3450	0.3240	0.3260	0.3780
Percentage improvement, %	6.1	3.7	1.3	−2.2	13.9	10.6	10.5	22.0
PCM + 5% CB_N234	0.1610	0.1430	0.1220	0.0910	0.3580	0.3450	0.3450	0.3730
Percentage improvement, %	8.4	5.9	3.4	−1.1	18.0	17.6	16.8	20.5

The results obtained indicate an improvement in thermal conductivity with the addition of carbon black, with the most pronounced enhancement observed for N234 carbon black. Therefore, further measurements were conducted for composites containing 2.5 and 5 wt.% of this nanoadditive. The average, in the temperature range of 25–55 °C, thermal conductivity improvement is 6.2% for PCM + 1% CB_N234, 11.7% for PCM + 2.5% CB_N234, and 17.4% for PCM + 5% CB_N234 as compared to the base PCM. The deviating value of the thermal conductivity at 70 °C can be attributed to the proximity of this temperature to the phase transition, which compromises the thermal equilibrium of the sample during measurement and results in anomalous thermal conductivity behavior.

A detailed description of the microscopic mechanisms of conductive heat transfer and heat transfer enhancement can be found in the work of Wu et al. [57]. In general, the role of CB particles in enhancing heat transfer can be attributed to the fact that, in organic PCMs, heat conduction occurs primarily through lattice vibrations, with phonons acting as the main carriers of thermal energy [58]. The presence of CB particles within the PCM provides additional pathways for phonon transport, thereby improving the effective thermal conductivity of the composite material [59]. However, poor dispersion of the additive and/or a too low mass fraction may prevent the formation of a continuous conductive network and may introduce thermal contact resistance, resulting in only a modest improvement in thermal conductivity [59]. Consequently, the literature suggests that only additive mass fractions exceeding a certain threshold—dependent on the type of PCM and the additive used—can effectively enhance thermal conductivity. The results obtained in the present study suggest that the threshold mass fraction of CB particles in the PCM is 1 wt.% or lower, as an improvement in thermal conductivity is already observed at this concentration. Nevertheless, further studies are required to evaluate thermal conductivity enhancement at even lower additive mass fractions.

PEW/CB systems offer superior advantages versus graphene and CNT: comparable thermal conductivity gains (18–22% vs. 15–30%) with significantly lower cost ($2–5/kg vs. $50–500/kg), making them industrially viable for large-scale thermal energy storage applications [14,60–62].

Figure 11A presents the temperature evolution curves of the investigated composites. The pure PCM sample does not exhibit a clear phase change transition; instead, only a small and nearly linear temperature increase is observed, reaching approximately 10 °C by the end of irradiation. Upon switching off the light source, an immediate temperature decrease occurs. In contrast, the composite samples show a rapid temperature rise from the onset of irradiation, accompanied by a characteristic inflection point associated with the phase change transition, particularly evident for the N220, N330, and N234 samples. This inflection point corresponds to the transition region in which the temperature increases at a reduced rate due to latent heat absorption during the phase change process.

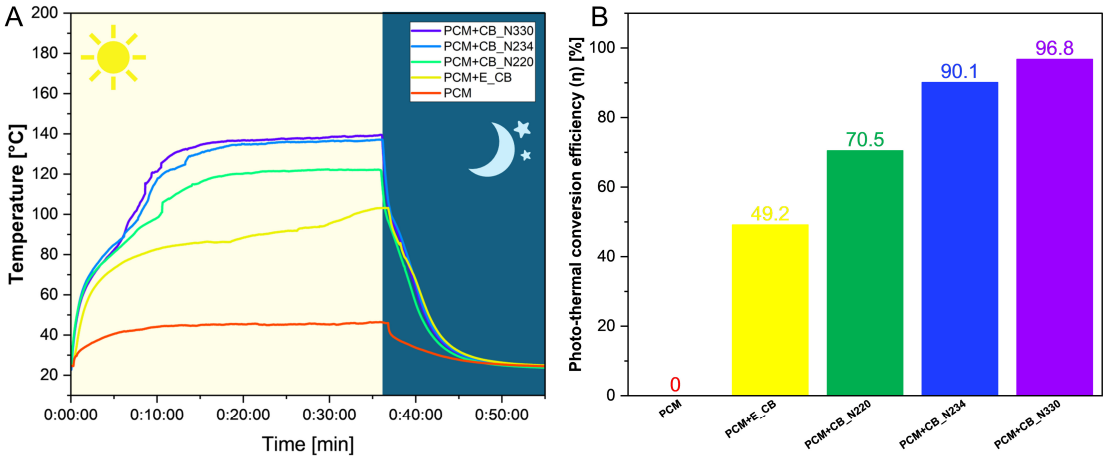

Figure 11. (**A**) Temperature evolution curves composites during solar–thermal conversion test, (**B**) calculated photothermal conversion efficiency.

The SE sample exhibited a rapid increase in temperature in the initial stage of irradiation; however, after reaching approximately 75 °C, the subsequent temperature increase was significantly lower compared to that of the N-series samples. In addition, this sample required a substantially longer irradiation time for the phase change transition to occur. The N330 and N234 samples showed the highest temperature increases, reaching approximately 135 °C within about 15 min. These values are high not only compared to the other samples studied here, but also relative to previously reported results [22,23]. Furthermore, the inflection point associated with the phase change transition appeared earlier and was shorter in duration for the N330 and N234 samples than for the N220 and SE samples. The thermal performance observed under the solar simulator is directly reflected in the photothermal conversion efficiency (Figure 11B). The highest photothermal conversion efficiencies were obtained for the N234 and N330 samples, resulting from their favorable combination of high thermal conductivity and high fusion enthalpy, determined by DSC measurements. In contrast, the SE and N234 samples exhibited lower photothermal conversion efficiencies, likely due to poorer light absorption and conversion performance. This behavior can be attributed to their lower thermal conductivity and the reduced enthalpy of melting observed in the DSC tests, possibly arising from less effective dispersion of the additive and the formation of agglomerates that hinder smooth phase transformation. Overall, the results confirm that carbon-based additives with strong optical absorption and adequate thermal conductivity are critical for optimizing photothermal performance in PEW-based composites. The N series formulations, particularly N330 and N234, demonstrate the best balance between absorption, heat generation, and controlled phase change

behavior, making them highly promising candidates for solar–thermal energy storage and conversion applications. In the literature, Luo X. et al. [60] used expanded graphite and carbon nanotubes to modify paraffin. Expanded graphite greatly improves the thermal conductivity of paraffin. Carbon black nanoparticles endow the paraffin satisfied light absorption capacity. The intrinsic photothermal conversion efficiency is up to 60.1% at 1000 W/m^2. Mishra et al. [26] examined that CBNP increases both conductivity and photothermal conversion by ~134% due to improved radiation absorption and the carbon scattering effect. In turn, Zhang et al. [63] show that composites with graphene foam can effectively convert light into heat, accumulating energy in the PCM and extending the heat release period. In a comprehensive review of carbon-based PCMs [64], the authors discuss various carbon additives (CNTs, CFs, graphene/rGO, expanded graphite, biocarbon) and their impact on solar-to-thermal conversion and other energy conversions. They point out that photothermal conversion in graphene/rGO-based PCMs typically exceeds that of simple carbon additives due to improved absorption and heat transfer networks.

4. Conclusions

This study presents a comprehensive evaluation of polyethylene wax–based phase change materials modified with seven distinct types of carbon black, focusing on their thermal behavior during phase transitions, thermal stability, microstructural characteristics, and photothermal performance. The results demonstrate that carbon black modification leads to modest reductions in the enthalpy of fusion (8–15% across the investigated formulations), which can be attributed to the space-occupying nature of the nanoparticles and their interference with the crystallization process of the PEW matrix. Importantly, the melting and solidification temperatures remained stable (95–96 °C), ensuring predictable thermal behavior and good reliability. Moreover, the ratio of solidification to melting enthalpy (Qs/Qm ≈ 0.90–0.98) confirms excellent thermal cycling performance, which is critical for reliable operation in practical mobile heating systems. Among the evaluated carbon black grades, N234 exhibited the most pronounced improvement in thermal conductivity, with a 6.8% enhancement at 1 wt.% loading at 25 °C and a 17.0% increase at 70 °C. These improvements directly translate into faster charging and discharging rates in thermal energy storage applications. Thermogravimetric analysis showed that all the systems investigated possess good thermal stability, with onset decomposition temperatures ($T_{1\%}$) in the range of 250–269 °C, well above the typical operating temperatures (90–100 °C) of mobile heating systems. SEM analysis revealed a uniform distribution of carbon black within the PEW matrix, with aggregate sizes in the range of 100 to 500 nm, characteristic of commercial carbon black products. Photothermal conversion experiments demonstrated particularly high efficiency for the N234 and N330 formulations, which exhibited rapid temperature increases, reaching approximately 135 °C within about 15 min under solar simulator irradiation. This performance can be attributed to the strong optical absorption of carbon black combined with enhanced thermal conductivity. Overall, the results confirm that carbon black is a viable and cost-effective additive for enhancing the thermal properties and photothermal conversion capability of PEW-based PCM systems, while maintaining excellent thermal stability and cycling performance. Consistent Tm and Ts values across all PCM/CB systems (95–96 °C and 90–91 °C, respectively) demonstrated strong thermal compatibility and the absence of interfacial chemical reactions, as it was confirmed in FTIR results. Analysis of the FTIR results for both neat PCM, PCM/CB samples, and CB indicates no changes in PEW in the presence of carbon black, which indicates no chemical reaction between the PCM and the carbon additive. DSC results after 20 heating–cooling cycles for the PCM base material and the two best formulations revealed that the best thermal

behavior and repeatability were exhibited by the PCM+CB_N330 sample, where the values of heat of phase transition were on a similar level as before thermal cycling.

Author Contributions: Conceptualization, M.S. and K.P.; methodology, M.S. and K.P.; formal analysis, M.S., P.S., K.S., E.R. and K.P.; investigation, M.S., P.S., K.S. and E.R.; data curation, M.S., P.S., K.S. and E.R.; writing—original draft preparation, M.S., P.S., E.R. and K.S.; writing—review and editing, M.S. and K.P.; visualization, M.S. and K.S.; supervision, K.P.; project administration, K.P.; funding acquisition, K.P. All authors have read and agreed to the published version of the manuscript.

Funding: The authors are grateful to the National Center for Research and Development for financial support under Contract No. NTE2/0004/2022 with the acronym MMC. This work was also supported by a subsidy from the Ministry of Science and Higher Education for the AGH University of Krakow (Project No. 16.16.160.557).

Data Availability Statement: The original contributions presented in this study are included in the article. Further inquiries can be directed to the corresponding author.

Conflicts of Interest: The authors declare no conflicts of interest.

References

1. Lawag, R.A.; Ali, H.M. Phase change materials for thermal management and energy storage: A review. *J. Energy Storage* **2022**, *55*, 105602. [CrossRef]
2. Pielichowska, K.; Szatkowska, M.; Pielichowski, K. Thermal Energy Storage in Bio-Inspired PCM-Based Systems. *Energies* **2025**, *18*, 3548.
3. Zhang, S.; Ocłoń, P.; Klemeš, J.J.; Michorczyk, P.; Pielichowska, K.; Pielichowski, K. Renewable energy systems for building heating, cooling and electricity production with thermal energy storage. *Renew. Sustain. Energy Rev.* **2022**, *165*, 112560. [CrossRef]
4. Zalba, B.; Marín, J.M.; Cabeza, L.F.; Mehling, H. Review on thermal energy storage with phase change: Materials, heat transfer analysis and applications. *Appl. Therm. Eng.* **2003**, *23*, 251–283. [CrossRef]
5. Pielichowska, K.; Pielichowski, K. Phase change materials for thermal energy storage. *Prog. Mater. Sci.* **2014**, *65*, 67–123. [CrossRef]
6. Mehling, H. Review of Classification of PCMs, with a Focus on the Search for New, Suitable PCM Candidates. *Energies* **2024**, *17*, 4455. [CrossRef]
7. Yang, G.; Yim, Y.J.; Lee, J.W.; Heo, Y.J.; Park, S.J. Carbon-Filled Organic Phase-Change Materials for Thermal Energy Storage: A Review. *Molecules* **2019**, *24*, 2055. [CrossRef]
8. Dash, L.; Mahanwar, P. A Review on Organic Phase Change Materials and Their Applications. *Int. J. Eng. Appl. Sci.* **2021**, *5*, 268–284.
9. Krupa, I.; Sobolčiak, P.; Abdelrazeq, H.; Ouederni, M.; Al-Maadeed, M.A. Natural aging of shape stabilized phase change materials based on paraffin wax. *Polym. Test.* **2017**, *63*, 567–572. [CrossRef]
10. Zauner, C.; Hengstberger, F.; Etzel, M.; Lager, D.; Hofmann, R.; Walter, H. Experimental characterization and simulation of a fin-tube latent heat storage using high density polyethylene as PCM. *Appl. Energy* **2016**, *179*, 237–246. [CrossRef]
11. Navarro, L.; Barreneche, C.; Castell, A.; Redpath, D.A.G.; Griffiths, P.W.; Cabeza, L.F. High density polyethylene spheres with PCM for domestic hot water applications: Water tank and laboratory scale study. *J. Energy Storage* **2017**, *13*, 262–267. [CrossRef]
12. Fikri, M.A.; Pandey, A.K.; Samykano, M.; Kadirgama, K.; George, M.; Saidur, R.; Selvaraj, J.; Abd Rahim, N.; Sharma, K.; Tyagi, V.V. Thermal conductivity, reliability, and stability assessment of phase change material (PCM) doped with functionalized multi-wall carbon nanotubes (FMWCNTs). *J. Energy Storage* **2022**, *50*, 104676. [CrossRef]
13. Feng, X.; Zhang, Y.; Yang, Z.; Zhao, Z.; Zhu, F.; Wei, X.; Chen, L.; Liu, J.; Feng, Y.; Li, C.; et al. Polyethylene glycol with dual three-dimensional porous carbon nanotube/diamond: A high thermal conductivity of composite PCM. *Nanotechnology* **2024**, *35*, 095702.
14. Mishra, A.K.; Ribezzo, A.; Morciano, M.; Bergamasco, L.; Campagnoli, E.; Giaretto, V.; Fasano, M.; Chiavazzo, E. Thermal conductivity enhancement in carbon black composite PCM for thermal energy storage. *J. Phys. Conf. Ser.* **2025**, *2940*, 012012.
15. Afaynou, I.; Faraji, H.; Choukairy, K.; Djebali, R.; Rezk, H. Comprehensive Analysis and Thermo-Economic Optimization of a Hybrid Phase Change Material-Based Heat Sink for Electronics Cooling. *Heat Transf.* **2025**, *54*, 3754–3774. [CrossRef]
16. Mishra, A.K.; Morciano, M.; Campagnoli, E.; Giaretto, V.; Fasano, M.; Chiavazzo, E. Coffee and turmeric bio-based shape-stabilized composite PCMs for thermal and solar energy storage applications. *Sol. Energy Mater. Sol. Cells* **2026**, *297*, 114136. [CrossRef]
17. Yu, J.; Feng, J. Form-stable phase change materials with enhanced thermal conductivity via segregated BN network within SEBS-supported paraffin wax for electronics thermal management. *Compos. Part A Appl. Sci. Manuf.* **2025**, *199*, 109187. [CrossRef]

18. Taylor, J.R. *An Introduction to Error Analysis: The Study of Uncertainties in Physical Measurements*; University Science Books: Melville, NY, USA, 1997.
19. Light Flash Apparatus LFA 467 HyperFlash® Series. 2026. Available online: https://analyzing-testing.netzsch.com/_Resources/Persistent/3/6/7/f/367f54b9bc7fc3a5b36f6b41191f5dbaf802ecb7/LFA_467_HyperFlash_en_web.pdf (accessed on 30 January 2026).
20. Analytical Balance. 2026. Available online: https://radwag.com/en/waga-analityczna-xa-82-220-5y,w1,9QF,114-107-100 (accessed on 30 January 2026).
21. Specific Heat Capacity Measurement. 2026. Available online: https://www.mt.com/be/nl/home/applications/Application_Browse_Laboratory_Analytics/Application_Browse_thermal_analysis/specific-heat-capacity-measurement.html (accessed on 30 January 2026).
22. Huang, Y.; Zou, M.; Chen, W.; Luo, W.; Hu, X.; Zhu, G.; Tan, S.; Jiang, X. A Novel Room-Temperature Flexible Phase Change Material for Solar Energy Photothermal Conversion and Battery Thermal Management. *ACS Sustain. Chem. Eng.* **2024**, *12*, 4662–4675. [CrossRef]
23. Cheng, G.; Wang, X.; He, Y. 3D graphene paraffin composites based on sponge skeleton for photo thermal conversion and energy storage. *Appl. Therm. Eng.* **2020**, *178*, 115560. [CrossRef]
24. Han, Z.; Zhao, Y.; Hu, S.; Zhou, Z.; Yan, Y.; Wang, C. Preparation and application of composite PCM with combined radiative cooling and photothermal conversion capabilities for building energy management. *Energy Build.* **2025**, *347*, 116363. [CrossRef]
25. Bharathiraja, R.; Ramkumar, T.; Selvakumar, M. Studies on the thermal characteristics of nano-enhanced paraffin wax phase change material (PCM) for thermal storage applications. *J. Energy Storage* **2023**, *73*, 109216. [CrossRef]
26. Mishra, A.K.; Lahiri, B.B.; Philip, J. Carbon black nano particle loaded lauric acid-based form-stable phase change material with enhanced thermal conductivity and photo-thermal conversion for thermal energy storage. *Energy* **2020**, *191*, 116572. [CrossRef]
27. Singh, R.P.; Sze, J.Y.; Kaushik, S.C.; Rakshit, D.; Romagnoli, A. Thermal performance enhancement of eutectic PCM laden with functionalised graphene nanoplatelets for an efficient solar absorption cooling storage system. *J. Energy Storage* **2021**, *33*, 102092. [CrossRef]
28. Fan, Z.; Zhao, Y.; Liu, X.; Shi, Y.; Jiang, D. Thermal Properties and Reliabilities of Lauric Acid-Based Binary Eutectic Fatty Acid as a Phase Change Material for Building Energy Conservation. *ACS Omega* **2022**, *7*, 16097–16108. [CrossRef] [PubMed]
29. Mishra, A.K.; Lahiri, B.B.; Philip, J. Effect of Surface Functionalization and Physical Properties of Nanoinclusions on Thermal Conductivity Enhancement in an Organic Phase Change Material. *ACS Omega* **2018**, *3*, 9487–9504. [CrossRef]
30. Colla, L.; Fedele, L.; Mancin, S.; Danza, L.; Manca, O. Nano-PCMs for enhanced energy storage and passive cooling applications. *Appl. Therm. Eng.* **2017**, *110*, 584–589. [CrossRef]
31. Rolka, P.; Lackowski, M. The effect of graphene nanoparticles on the thermal conductivity enhancement of organic phase change material and its energy storage properties. *Arch. Thermodyn.* **2024**, *44*, 103–121.
32. Diby, I.C.P.; Belkhiri, N.; Nohair, B.; Kazeruni, M.; Ruiz, E.; Kaliaguine, S. HDPE crystalline lamellae in composites involving pyrolytic carbon black: Effect on elastic modulus. *Polym. Compos.* **2025**, *46*, 38–53.
33. Spahr, M.E.; Rothon, R. Carbon Black as a Polymer Filler. In *Fillers for Polymer Applications*; Springer: Cham, Switzerland, 2017; pp. 261–291.
34. Fredi, G.; Dorigato, A.; Fambri, L.; Pegoretti, A. Wax Confinement with Carbon Nanotubes for Phase Changing Epoxy Blends. *Polymers* **2017**, *9*, 405. [CrossRef]
35. Pasupathi, M.K.; Alagar, K.; Stalin, P.M.J.; Matheswaran, M.M.; Aritra, G. Characterization of Hybrid-nano/Paraffin Organic Phase Change Material for Thermal Energy Storage Applications in Solar Thermal Systems. *Energies* **2020**, *13*, 5079. [CrossRef]
36. Ahmad, I.A.; Kim, H.K.; Deveci, S.; Kumar, R.V. Non-Isothermal Crystallisation Kinetics of Carbon Black- Graphene-Based Multimodal-Polyethylene Nanocomposites. *Nanomaterials* **2019**, *9*, 110. [CrossRef] [PubMed]
37. Yadav, D.K.; Rathore, P.K.S.; Singh, R.K.; Gupta, A.K.; Sikarwar, B.S. Experimental Study on Paraffin Wax and Soya Wax Supported by High-Density Polyethylene and Loaded with Nano-Additives for Thermal Energy Storage. *Energies* **2024**, *17*, 2461. [CrossRef]
38. Sharma, A.; Singh, P.K.; Sharma, K. Synergistic Effects of Heated Walnut Shell Powder and Reduced Graphene Oxide in Paraffin Wax Composites for Marine Thermal Applications. *Int. J. Marit. Eng.* **2024**, *1*, 277–286. [CrossRef]
39. Nejman, A.; Gromadzińska, E.; Kamińska, I.; Cieślak, M. Assessment of Thermal Performance of Textile Materials Modified with PCM Microcapsules Using Combination of DSC and Infrared Thermography Methods. *Molecules* **2019**, *25*, 122. [CrossRef]
40. Sun, X.; Lee, K.O.; Medina, M.A.; Chu, Y.; Li, C. Melting temperature and enthalpy variations of phase change materials (PCMs): A differential scanning calorimetry (DSC) analysis. *Phase Transit.* **2018**, *91*, 667–680.
41. Kumari, P.; Raj, A.; Ghosh, D. Selection of Phase Change Material for Latent Heat Thermal Energy Storage Using a Hairpin Heat Exchanger: Numerical Study. *J. Therm. Sci. Eng. Appl.* **2024**, *16*, 091005. [CrossRef]
42. Nazari, S.M.; Caggiano, A.; Mankel, C.; Koenders, E. A Comparative Study on the Thermal Energy Storage Performance of Bio-Based and Paraffin-Based PCMs Using DSC Procedures. *Materials* **2020**, *13*, 1705. [CrossRef]
43. Mane, N.S.; Kodancha, P.; Hemadri, V.; Tripathi, S. Investigation on Cooling Performance of Composite PCM and Graphite Fin for Battery Thermal Management System of Electric Vehicles. *Energy Storage* **2024**, *6*, e70024. [CrossRef]

44. Dogan, O.M.; Keskin, S.; Dogan, A.; Ataman, H.; Usanmaz, A. Structure-property Relation of a Soft Liner Material Used in Denture Applications. *Dent. Mater. J.* **2007**, *26*, 329–334. [CrossRef] [PubMed]
45. Zhuang, J.; Li, M.; Pu, Y.; Ragauskas, A.; Yoo, C. Observation of Potential Contaminants in Processed Biomass Using Fourier Transform Infrared Spectroscopy. *Appl. Sci.* **2020**, *10*, 4345. [CrossRef]
46. Bacher, D.A. Infrared Spectroscopy n.d. Available online: https://webspectra.chem.ucla.edu/irtable.html (accessed on 6 September 2024).
47. Kim, H.B.; Mae, M.; Choi, Y. Thermal Performance Measurement Procedure and Its Accuracy for Shape-Stabilized Phase-Change Material and Microcapsule Phase-Change Material Combined with Building Materials. *Sustainability* **2021**, *13*, 6671. [CrossRef]
48. Öner, G.A. Flexural strength and thermal properties of carbon black nanoparticle reinforced epoxy composites obtained from waste tires. *Open Chem.* **2022**, *20*, 863–872. [CrossRef]
49. Yu, J.; Li, H.; Kong, L.; Zhu, H.; Zhu, Q.; Wang, H. Effects of Nanofilled Particle Forms and Dispersion Modes on Properties of Carbon-Based Energy Storage Composites. *Adv. Polym. Technol.* **2020**, *2020*, 6865497. [CrossRef]
50. Laghari, I.A.; Pandey, A.K.; Samykano, M.; Aljafari, B.; Kadirgama, K.; Sharma, K.; Tyagi, V.V. Thermal energy harvesting of highly conductive graphene-enhanced paraffin phase change material. *J. Therm. Anal. Calorim.* **2023**, *148*, 9391–9402. [CrossRef]
51. Singh, M.; Vander Wal, R.L. Nanostructure Quantification of Carbon Blacks. *C* **2018**, *5*, 2. [CrossRef]
52. Almousa, N.H.; Alotaibi, M.R.; Alsohybani, M.; Radziszewski, D.; AlNoman, S.M.; Alotaibi, B.M.; Khayyat, M.M. Paraffin Wax [As a Phase Changing Material (PCM)] Based Composites Containing Multi-Walled Carbon Nanotubes for Thermal Energy Storage (TES) Development. *Crystals* **2021**, *11*, 951. [CrossRef]
53. Feng, L.; Wu, J.; Sun, W.; Cai, W. Effects of Pore Structure and Pore Size of Expanded Graphite on the Properties of Paraffin Wax/Expanded Graphite Composite Phase Change Materials. *Energies* **2022**, *15*, 4201. [CrossRef]
54. Aslan, O.; Atalar, T.; Yılmaz, G.A.; Özkan, N. Enhancing the performance of HTPB-IPDI-based polyurethane composite liner through effective carbon black dispersion. *Propell. Explos. Pyrotech.* **2023**, *48*, e202300107. [CrossRef]
55. Samuel, J.; Yussuf, A.A.; Al-Zufairi, R.; Al-Banna, A.; Al-Shammary, T.; Abraham, G. High density polyethylene hybrid nanocomposites reinforced with carbon nanofiber and nanoclay. *J. Elastomer Plast.* **2024**, *56*, 713–731. [CrossRef]
56. Fan, R.; Wan, M.; Zheng, N.; Sun, Z. Simultaneously enhanced light absorption and heat transfer capability of melamine foam stabilized phase change composites by carbon black and metal fins for photothermal conversion and storage. *J. Energy Storage* **2022**, *54*, 105278. [CrossRef]
57. Wu, S.; Yan, T.; Kuai, Z.; Pan, W. Thermal conductivity enhancement on phase change materials for thermal energy storage: A review. *Energy Storage Mater.* **2020**, *25*, 251–295. [CrossRef]
58. Li, Z.R.; Hu, N.; Fan, L.W. Nanocomposite phase change materials for high-performance thermal energy storage: A critical review. *Energy Storage Mater.* **2023**, *55*, 727–753.
59. Cheng, P.; Chen, X.; Gao, H.; Zhang, X.; Tang, Z.; Li, A.; Wang, G. Different dimensional nanoadditives for thermal conductivity enhancement of phase change materials: Fundamentals and applications. *Nano Energy* **2021**, *85*, 105948. [CrossRef]
60. Luo, X.; Hao, B.; Xiang, H.; Li, H.; Tao, Z. A novel phase change materials used for direct photothermal conversion and efficient thermal storage. *Sol. Energy Mater. Sol. Cells* **2023**, *251*, 112142. [CrossRef]
61. Leong, K.Y.; Hasbi, S.; Ku, A.K.Z.; Mat, J.N.; Ong, H.C.; Din, M.F. Thermal properties evaluation of paraffin wax enhanced with carbon nanotubes as latent heat thermal energy storage. *J. Energy Storage* **2022**, *52*, 105027. [CrossRef]
62. Lu, X.; Liu, H.; Murugadoss, V.; Seok, I.; Huang, J.; Ryu, J.E.; Guo, Z. Polyethylene Glycol/Carbon Black Shape-Stable Phase Change Composites for Peak Load Regulating of Electric Power System and Corresponding Thermal Energy Storage. *Eng. Sci.* **2020**, *9*, 25–34. [CrossRef]
63. Zhang, L.; Li, R.; Tang, B.; Wang, P. Solar-thermal conversion and thermal energy storage of graphene foam-based composites. *Nanoscale* **2016**, *8*, 14600–14607. [CrossRef]
64. Chen, X.; Cheng, P.; Tang, Z.; Xu, X.; Gao, H.; Wang, G. Carbon-Based Composite Phase Change Materials for Thermal Energy Storage, Transfer, and Conversion. *Adv. Sci.* **2021**, *8*, 2001274. [CrossRef]